Current Biology 23, 2016–2022, October 21, 2013 ©2013 Elsevier Ltd All rights reserved http://dx.doi.org/10.1016/j.cub.2013.08.033

Report

Striated Rootlet and Nonfilamentous Forms of Rootletin Maintain Ciliary Function

Swetha Mohan,[1] Tiffany A. Timbers,[1] Julie Kennedy,[2] Oliver E. Blacque,[2] and Michel R. Leroux[1,*]
[1]Department of Molecular Biology and Biochemistry, Simon Fraser University, Burnaby, BC V5A 1S6, Canada
[2]School of Biomolecular and Biomedical Science, UCD Conway Institute, University College Dublin, Belfield, Dublin 4, Ireland

Summary

Primary cilia are microtubule-based sensory organelles whose structures and functions must be actively maintained throughout animal lifespan to support signal transduction pathways essential for development and physiological processes such as vision and olfaction [1]. Remarkably, few cellular components aside from the intraflagellar transport (IFT) machinery are implicated in ciliary maintenance [2]. Rootletin, an evolutionarily conserved protein found as prominent striated rootlets or a nonfilamentous form, both of which are associated with cilium-anchoring basal bodies, represents a likely candidate given its well-known role in preventing ciliary photoreceptor degeneration in a mouse model [3, 4]. Whether rootletin is universally required for maintaining ciliary integrity, and if so, by what mechanism, remains unresolved. Here, we demonstrate that the gene disrupted in the previously isolated *C. elegans* chemosensory mutant *che-10* encodes a rootletin ortholog that localizes proximally and distally to basal bodies of cilia harboring or lacking conspicuous rootlets. In vivo analyses reveal that CHE-10/rootletin maintains ciliary integrity partly by modulating the assembly, motility, and flux of IFT particles, which are critical for axoneme length control. Surprisingly, CHE-10/rootletin is also essential for stabilizing ciliary transition zones and basal bodies, roles not ascribed to IFT. Unifying these findings, we provide evidence that the underlying molecular defects in the *che-10* mutant stem from disrupted organization/function of the periciliary membrane, affecting the efficient delivery of basal body-associated and ciliary components and resulting in cilium degeneration. Together, our cloning and functional analyses of *C. elegans che-10* provide the first mechanistic insights into how filamentous and nonfilamentous forms of rootletin play essential roles in maintaining ciliary function in metazoans.

Results

The *C. elegans* Rootletin Ortholog, CHE-10, Localizes at the Proximal and Distal Ends of Basal Bodies

To enlighten the process of cilium formation and/or maintenance, we sought to analyze the molecular function of the *che-10* gene, which encodes an ~230 kDa rootletin ortholog (Figure 1A; see also Figure S1A available online). Using transmission electron microscopy (TEM), Perkins et al. showed that the *che-10(e1809)* chemosensory mutant lacked most amphid (head) cilia and the cytoskeleton-like structure, striated rootlets [5]. Another allele, *dyf-14(ks69)*, was later found to possess ciliary defects identifiable via a protein marker for intraflagellar transport (IFT) [6, 7], a process that mobilizes ciliary precursors from the base of cilia to the growing end of the ciliary axoneme [8, 9].

We identified a nonsense mutation in *che-10(e1809)* and confirmed that it lacks the CHE-10 protein (Figures 1A and S1A). Notably, our finding agrees with loss of striated rootlets from this mutant [5]. Like *dyf-14(ks69)* [6], we show that *che-10(e1809)* and a third allele, *m525* [10], exhibit chemosensory (osm) and dye-filling (dyf) anomalies, consistent with structurally impaired cilia (Figures 1B and S1B–S1D). Wild-type worms incorporate dye (through intact, environmentally exposed cilia) in twelve amphid and four phasmid (tail) neurons, but *che-10(e1809)* mutants uptake dye in only two to four amphid and no phasmid neurons (Figure S1C). As *che-10(e1809)* mutants develop, fewer sensory neurons dye fill; whereas all L1 larvae incorporate dye in two to four amphid neurons, only 20% L4 larvae and no adults dye fill (Figure 1B). Importantly, a fosmid harboring wild-type *che-10* rescues the chemosensory and dye-filling defects (Figures S1B and S1C). Together, these findings confirm that *che-10* ciliary defects result from disrupting rootletin, with the progressively penetrant *dyf* phenotype suggesting that cilia degenerate over time.

Given that striated rootlets in *C. elegans* hermaphrodites exist in only three ciliated neuron types (IL1, OLQ, and BAG), we were surprised that abrogating CHE-10/rootletin affects nearly all ciliated cells [5]. Intriguingly, an electron-dense "amorphous root" near basal body (BB)-associated transition fibers was reported, but its significance was unexplored [5]. We therefore queried whether CHE-10 functions at the base of all cilia, irrespective of their association with rootlets. Indeed, full-length GFP-tagged CHE-10 localizes at proximal ends of all BBs, which are marked (together with ciliary axonemes) by the IFT protein XBX-1 (Figure 1C). Interestingly, CHE-10 is also present at the proximalmost (transition zone [TZ]) region of the axoneme, a novel observation potentially relevant to the ciliary degeneration phenotype (see below).

Our findings are the first demonstration—in any organism—that rootletin influences the integrity of cilia without prominent rootlets. This may be relevant to mammalian cilia, because many cell types, including olfactory neurons resembling *C. elegans* chemosensory neurons, lack discernible rootlets but possess rootletin puncta/accumulations near their basal bodies [4, 11]. Surprisingly, however, neurons whose striated rootlets are lost in the *C. elegans che-10* mutant possess seemingly intact cilia through to adulthood [5]. Based on experimental results presented in a later section, we suspect that these cilia do degenerate, albeit more slowly.

Maintenance of Ciliary Structure during Development Requires CHE-10/Rootletin

To confirm our hypothesis that *che-10* mutant cilia degenerate rather than fail to form, we observed the GFP-tagged IFT kinesin OSM-3 throughout development (Figure 1D). In *che-10* mutants, ~20% of L2/L3 larvae, and no L4 larvae or

*Correspondence: leroux@sfu.ca

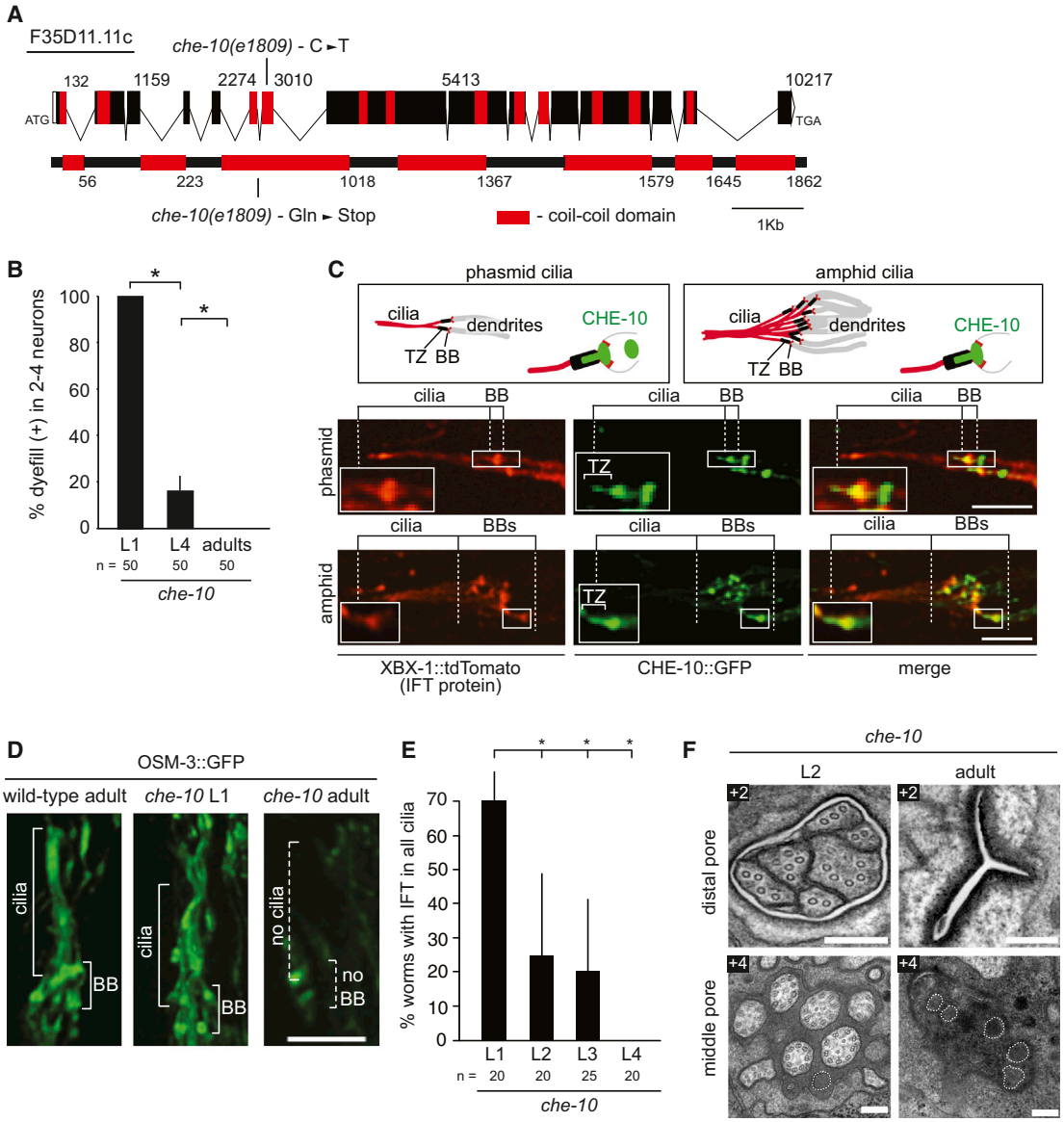

Figure 1. *C. elegans che-10* Encodes a Rootletin Ortholog that Localizes Proximally to Basal Bodies and within the Transition Zone and Is Required for Ciliary Maintenance during Development

(A) Genomic structure of *che-10*, domain structure of the protein, and position of the *e1809* allele (Gln_{371}-to-stop nonsense mutation). See also Figure S1A.

(B) Fluorescent dye filling of two to four ciliated neurons is progressively lost from *che-10* L1 larvae to adults, consistent with cilia structure defects. Fisher's exact test for significance, $p < 0.01$. Error bars represent 95% confidence intervals (Clopper-Pearson method for binomial data). See also Figures S1C and S1D.

(C) CHE-10 localizes at the basal body (BB) proximal ends and within transition zone (TZ) regions. CHE-10::GFP is shown together with XBX-1::tdTomato, which marks BBs and transition fibers (TFs). Schematics show relative positions of the proteins with respect to cilia, BBs/TFs, TZs, and axonemes in head (amphid) and tail (phasmid) neurons. Scale bar represents 5 μm.

(D) Amphid cilia, marked by OSM-3::GFP, are present and display IFT in *che-10* L1 larvae but are absent in adults and show no discernible BBs or OSM-3 within cilia. Scale bar represents 5 μm.

(E) Quantitation of OSM-3::GFP in amphid channel cilia throughout development. Approximately 70% L1 larvae have cilia displaying IFT, whereas only ~20% L2/L3 and no L4 larvae exhibit IFT. Fisher's exact test for significance, $p < 0.01$. Error bars represent 95% confidence intervals (Clopper-Pearson method for binomial data).

(F) Ultrastructure of amphid pore in *che-10* mutants. Shown are representative TEM images from serial cross-sections taken from L2 larval and young adult stages. Boxed number denotes proximal position of section (in μm) relative to the first section in the series. Dashed outlines denote "ghost axonemes," presumably representing degenerated cilia. Scale bars represent 200 nm.

adults, have amphid cilia (Figure 1E). In contrast, ~70% of *che-10* L1 larvae possess amphid cilia, and occasionally phasmid cilia are visible; furthermore, OSM-3 accumulations at dendritic tips are rarely observed, and IFT is grossly wild-type (Figures 1D and 1E; Movie S1). This demonstrates that ciliogenesis occurs in *che-10* mutants, although by the L1 stage, amphid cilia are shorter, causing a dye-fill defect (Figure 1B).

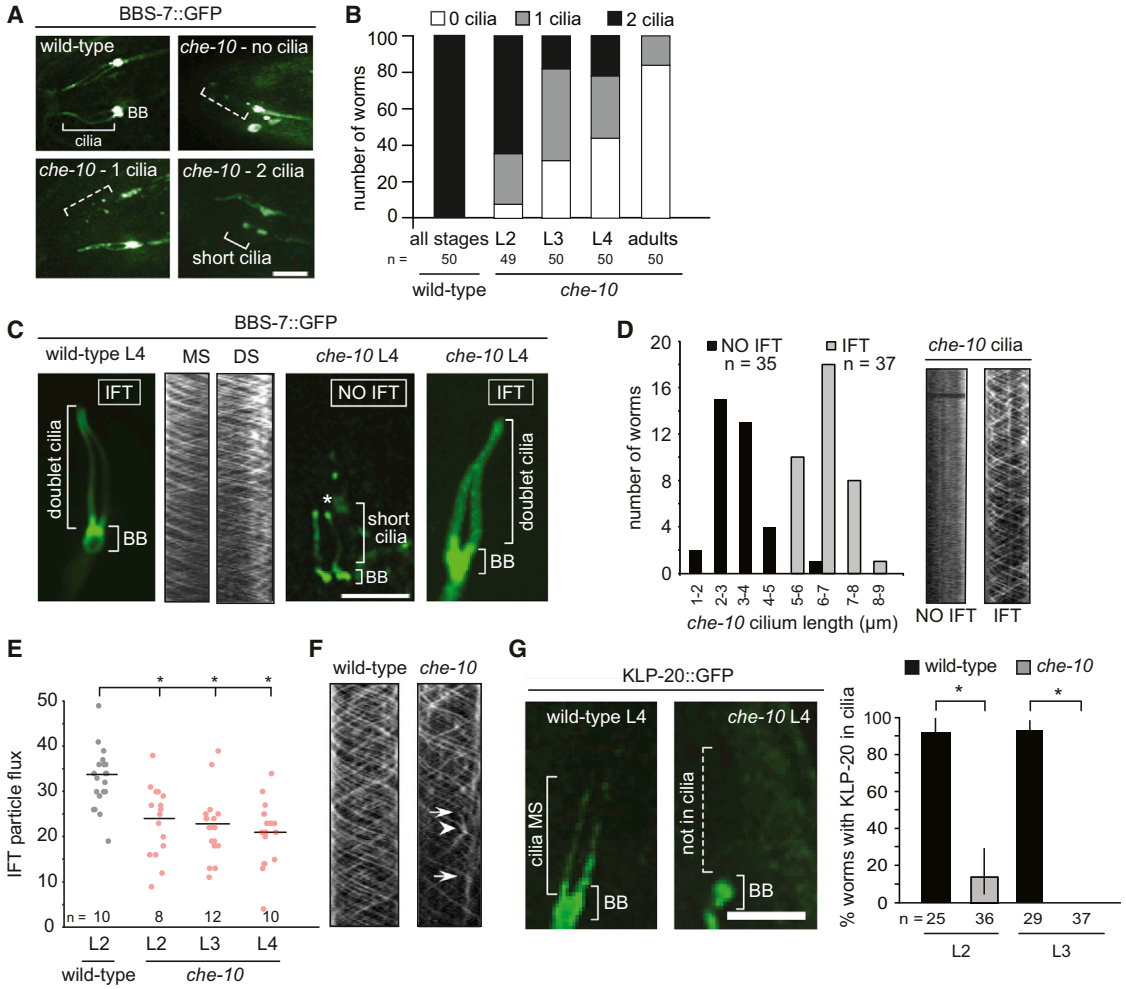

Figure 2. CHE-10/Rootletin Is Required for Normal Intraflagellar Transport

(A) ADL doublet cilia degenerate during development. Representative images are shown of wild-type ADL doublet cilia (all have two) and *che-10* ADL doublet cilia (zero to two are observed) marked by BBS-7::GFP. Scale bar represents 5 μm. See also Figure S1E.

(B) Quantitation of ADL cilia number throughout development. In *che-10* mutants, more worms in early development have both doublet cilia (~60%) as compared to L4 larvae (~20%) and adults (none). Fisher's exact test for significance, $p < 0.01$. See also Figure S1F.

(C) *che-10* mutants possess short cilia that fail to exhibit IFT. BBS-7::GFP expressed in ADL neurons localizes to BBs and ciliary axonemes. IFT in wild-type middle segments (MSs) and distal segments (DSs) is shown as kymographs. *che-10* ADL cilia range from short (left panel) and devoid of IFT to wild-type length (right panel); longer *che-10* cilia display IFT, whereas shorter cilia do not and have accumulations (*) at the tip. Scale bar represents 5 μm. See also Figure S1G.

(D) Quantitation of ciliary length and presence/absence of BBS-7::GFP IFT in *che-10* mutants. *che-10* cilia < 5 μm in length lack IFT, whereas cilia > 5 μm and closer to wild-type length display IFT, as revealed by kymograph analysis. Student's t test for significance, $p < 0.01$. See also Figure S1G.

(E) Quantitation of IFT flux in *che-10* mutants compared to wild-type. Graph reveals a statistically significant reduction in anterograde IFT particle flux in ADL cilia of *che-10* worms (~20–25 particles/doublet cilium × min) compared to wild-type (~35). Student's t test for significance, $p < 0.01$. See also Figure S2B.

(F) Representative kymographs of BBS-7::GFP undergoing IFT in ADL cilia. Wild-type larvae exhibit smooth anterograde and retrograde transport. *che-10* mutant kymograph shows unstable movements, including stalling (arrowhead) and stopping (arrows).

(G) Defect in kinesin II subunit (KLP-20) ciliary entry in *che-10* mutant. Approximately 90% of wild-type L2 and L3 larvae show KLP-20 undergoing IFT in the MS, whereas only ~20% of *che-10* L2 larvae and no L3 larvae incorporate kinesin II within cilia. Fisher's exact test for significance, $p < 0.01$. Error bars represent 95% confidence intervals (Clopper-Pearson method for binomial data). BB, basal body. Scale bar represents 5 μm.

Our TEM analyses of amphid cilia support this observation. *che-10* mutant L2 larvae display four to five grossly intact axonemes, and frequently the ciliary subcompartments (TZ, middle segments, and distal segments [MSs and DSs, respectively]) are intact (Figure 1F; Table S1). In contrast, *che-10* young adults possess only one or two seemingly intact axonemes (potentially ADF/ADL double-rod cilia), with some amphid pores devoid of ciliary structures (Figure 1F; Table S1; see also [5] for adult TEMs). In L2 larvae and adults, electron-dense "ghost" structures suggestive of microtubules, likely representing degenerating axonemes, are visible (Figure 1F; Table S1).

To study the degeneration process, we examined ADL cilia, whose neurons incorporate dye presumably through intact cilia (Figure S1E). GFP-tagged IFT markers (BBS-7, IFT-20, and dynein subunit XBX-1/DLIC) were introduced in ADL neurons (Figures 2A and S1F). In all cases, both ADL doublet cilia were more prevalent in *che-10* L2 larvae (~65%) compared to adults (0%) (Figures 2A and S1F), consistent with reduced ADL dye fill during development. Furthermore,

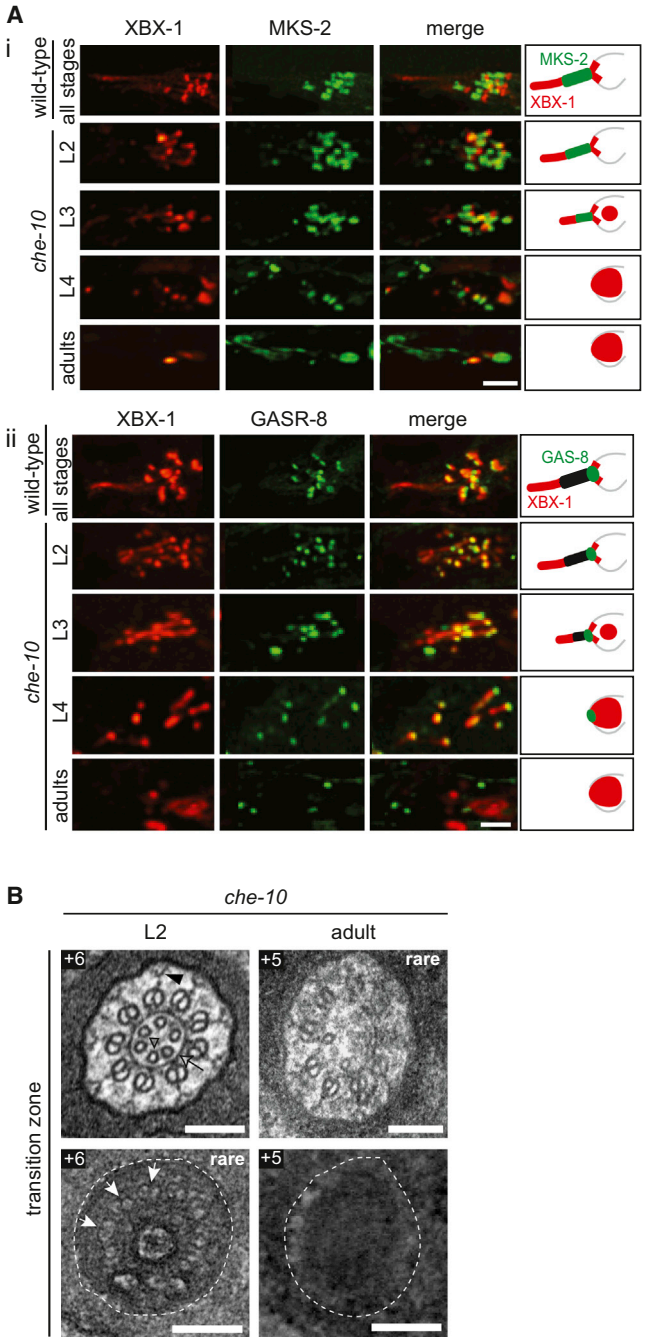

Figure 3. CHE-10/Rootletin Maintains the Integrity of the Transition Zone and Basal Body/Transition Fibers

(A) Structural integrity of the ciliary base throughout development. See also Figure S2C. Scale bar represents 5 μm.

(Ai) The TZ is marked by MKS-2::GFP, and the IFT comarker XBX-1::tdTomato marks the BB/TFs and cilia. In *che-10* mutants, MKS-2 localizes to the TZ until L3 larvae. In L4 larva, the TZ markers are absent, indicating TZ degeneration. Scale bar represents 5 μm.

(Aii) BB/TFs are marked by GASR-8::GFP, and XBX-1::tdTomato marks BB/cilia. GASR-8 localizes to BB/TFs in *che-10* mutants until L4 larvae but is absent in adults, consistent with BB/TF degeneration. Scale bar represents 5 μm.

(B) Ultrastructure of TZ compartment in amphid channel cilia of *che-10* mutants. Shown are representative TEM images from serial cross-sections taken from L2 larval and young adult stages. Boxed number denotes proximal position of section (in μm) relative to the first section. Arrow indicates apical ring; closed black arrowhead indicates Y links; open arrowhead indicates inner microtubules; closed white arrows indicate microtubule doublets. Scale bars represent 100 nm. See also Table S1.

compared to wild-type worms, whose cilia are 6–9 μm long, *che-10* mutant cilia are highly variable in length, from essentially wild-type to very short cilia (~2–9 μm) (Figure S1G).

Hence, cilia lacking striated rootlets progressively degenerate in worms lacking CHE-10/rootletin, similar to the slow ciliary photoreceptor degeneration phenotype observed for the mouse rootletin knockout [12]. But what is the molecular basis of this defect? Rootletin binds kinesin light chain 3 (KLC3) [13], suggesting that it acts as a docking site for cilium-targeted vesicular trafficking. It also interacts with the exocytosis machinery components SNAP-25, secretagogin, and ARFGAP2 [14], hinting that it may assist vesicle fusion/docking at the periciliary membrane. Finally, rootletin binds and may help organize the actin cytoskeleton at the ciliary base [12]; because actin also interacts with the exocyst complex and facilitates vesicle fusion with the apical membrane [15], such a function may be critical for delivering ciliary cargo at the periciliary membrane.

CHE-10/Rootletin Regulates Intraflagellar Transport

To test our hypothesis that CHE-10/rootletin may affect "late" stages of ciliary protein delivery, we first focused on the IFT machinery, which is trafficked to the ciliary base and represents a key contributor to cilium length control and maintenance [2]. We wondered whether variable ADL cilia lengths observed in *che-10* mutants (Figure S1G) correlate with IFT dysfunction. Strikingly, time-lapse imaging and kymograph analyses revealed that only *che-10* ADL cilia > 5 μm in length undergo IFT (Figures 2C and 2D; Movies S2, S3, and S4). This suggested that CHE-10 maintains ciliary integrity at least partly by modulating IFT. To test this, we compared velocity profiles of IFT-associated BBS-7 in wild-type and *che-10* ADL cilia (Figure S2A). Anterograde IFT particles normally move at ~0.7 μm/s in ciliary MSs, consistent with kinesin II and OSM-3-kinesin motors working in coordination, and ~1.2 μm/s in DSs, with OSM-3 operating alone (Figure S2A; Movie S2) [16, 17]. In contrast, as *che-10* animals develop, the MS exhibits progressively more faster-moving BBS-7 particles, whereas the DS displays an increase in slower-moving particles: the overlap between MS/DS velocities observed in *che-10* mutants is similar to wild-type (31% versus 40%) in L2 larvae but increases (94%) in L4 larvae (Figure S2A). *che-10* mutants also exhibit decreased IFT particle flux (~20–25 particles/min compared to ~35 in wild-type) (Figure 2E) and erratic IFT, including stalling and stopping (Figure 2F). Notably, wild-type and *che-10* worms display a correlation between cilium length and IFT particle flux, unlike that reported in *Chlamydomonas* [18]. However, reduced flux in *che-10* mutants is apparent in cilia of wild-type length, suggesting reduced IFT particle delivery independent of cilium length (Figure S2B). Hence, CHE-10/rootletin is required for wild-type IFT behavior/function, and our results suggest an influence on motor coordination/function, perhaps via IFT particle delivery and/or assembly at the ciliary base (periciliary membrane).

We next examined the transport kinetics of the ciliary motors KLP-20 (kinesin II subunit) and XBX-1/DLIC (IFT-dynein subunit) in ADL neurons. Similar to OSM-3-kinesin (Figure 1D), XBX-1 enters ADL cilia and undergoes IFT (data not shown;

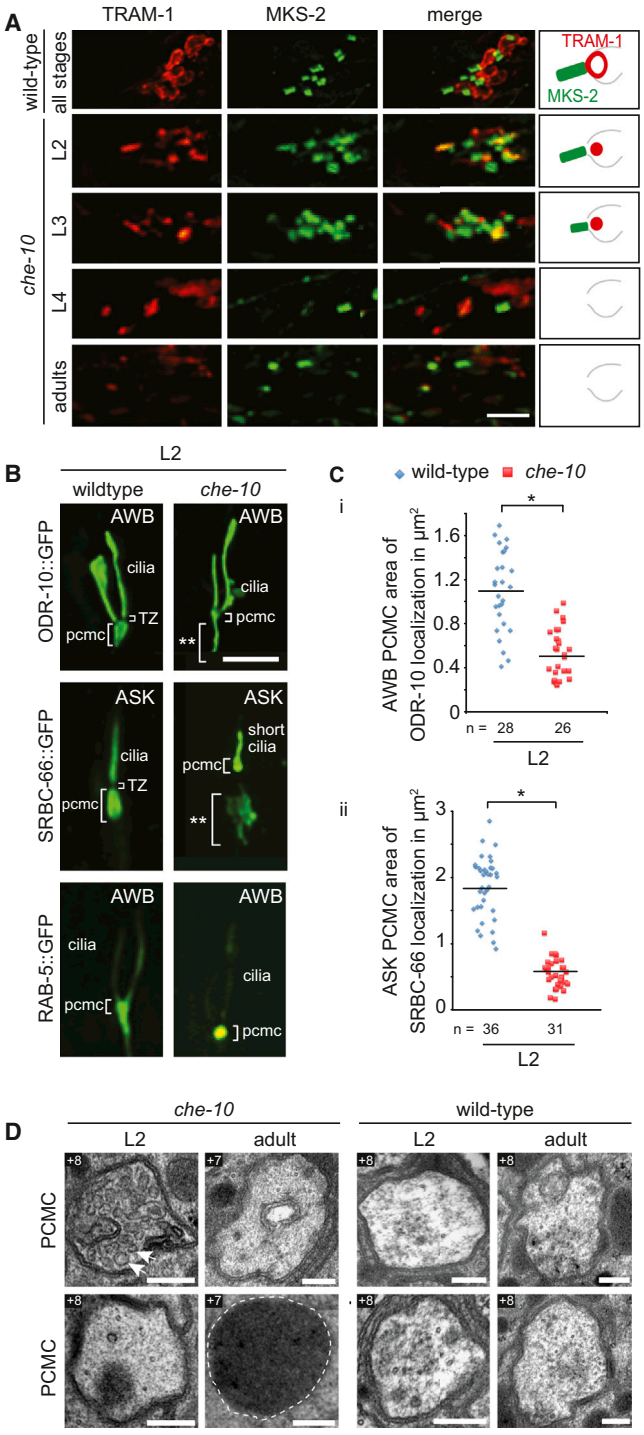

Figure 4. CHE-10 Regulates the Organization and Function of the Periciliary Membrane Compartment

(A) The PCMC is marked by TRAM-1::tdTomato, and MKS-2 marks the TZ. Unlike wild-type worms, TRAM-1 does not localize to the periciliary membrane compartment (PCMC) in *che*-10 L2 larvae. Scale bar represents 5 μm. See also Figure S2C.

(B) ODR-10, SRBC-66, and RAB-5 show altered localization at the PCMC in L2 larvae of *che-10* mutants compared to wild-type. ODR-10::GFP and SRBC-66::GFP localize to a smaller PCMC area and show accumulations proximal to it (denoted by **); RAB-5::GFP shows more concentrated localization to the PCMC and reduced signal within cilia. TZ, transition zone. Scale bar represents 5 μm.

(Ci and Cii) Quantification of area occupied by proteins within the PCMC area in an AWB neuron, marked by ODR-10 (Ci), and an ASK neuron, marked by SRBC-66 (Cii). *che-10* L2 larva mutants show a smaller area of protein localization at the PCMC in AWB and ASK neurons compared to wild-type. Student's t test for significance, $p < 0.01$.

(D) Ultrastructure of PCMC in amphid channel cilia of wild-type and *che-10* animals. Shown are representative TEM images from serial cross-sections taken from L2 larval and young adult stages. Boxed number denotes proximal position of section (in μm) relative to the first section in the series. Arrows indicate membranous accumulation. Scale bars represent 200 nm. See also Table S1.

Figure S1F). Remarkably, KLP-20 entry is severely compromised in *che-10* mutants (Figure 2G). Although KLP-20 undergoes IFT in ~90% wild-type L2/L3 larvae, significantly fewer (~20%) L2 and no L3 larvae showed KLP-20 in ADL cilia MSs of *che-10* mutants (Figure 2G). Because it is not incorporated into IFT trains, we hypothesize that KLP-20 may not be delivered to or assembled at the periciliary membrane, proximal to IFT docking sites (transition fibers). Progressive loss of kinesin II function partly explains the IFT anomalies of *che-10* cilia; other changes (e.g., assembly defects) in IFT machinery may collectively explain other phenotypes (velocity changes, stalling, and stopping). Thus, CHE-10/rootletin is required for the proper assembly and function of the IFT machinery, and we correlate defects in this process with axonemal degeneration.

Transition Zone and Basal Body Integrity Depend on CHE-10/Rootletin

To further dissect the role of CHE-10/rootletin on cilium maintenance, we monitored the integrity of the TZ and BB during development. Two well-established TZ markers, NPHP-1 and MKS-2, appeared intact in early larval stages (L2/L3) but were lost by the L4 stage (Figures 3Ai and S2Ci; data not shown for NPHP-1). This finding may be relevant to CHE-10 localization at both BBs and TZs (Figure 1C). TEM analyses confirmed that amphid channel pores in *che-10* L2 larvae have grossly intact TZs; in contrast, TZs were lacking in several pores in young adult *che-10* worms (Figure 3B; Table S1).

To assess BB integrity, we employed GASR-8 (Gas8 ortholog) as a marker, as it localizes specifically to BBs/TFs in *C. elegans* (Figures 3Aii and S2Cii; V.L. Jensen, personal communication). In *che-10* mutants, GASR-8::GFP is enriched at BBs until the L4 larval stage but lost in adults. Significantly, progressive disruption of TZ-BB structures in *che-10* mutants is not observed in IFT mutants, wherein most of the axoneme is not built [5, 19]. Thus, over time, disrupting CHE-10/rootletin has a surprisingly greater impact on BB-ciliary integrity than abrogating IFT—implying that defective IFT is unlikely to be the primary molecular defect in *che-10* animals.

CHE-10/Rootletin Maintains Periciliary Membrane Integrity

Given that TZs and BBs degenerate in *che-10* mutants, we hypothesized that the integrity of the periciliary membrane compartment (PCMC)—which makes connections to the BB via TFs and is the site of IFT particle docking and assembly [20]—is likely compromised, leading to inefficient delivery of ciliary components, including TZ, BB, and IFT proteins. To test this hypothesis, we employed TRAM-1, a PCMC marker [19, 20]. TRAM-1 exists at the ciliary base of wild-type worms throughout development but remarkably is largely lost in L2 larvae (when TZs and BBs are still intact) and absent from L4/adult stages in *che-10* mutants (Figures 4A and S2Ciii).

To provide additional evidence for PCMC disruption in *che-10* mutants, we examined two GPCRs, ODR-10 and SRBC-66, which localize at PCMCs and cilia of wild-type AWB and ASK neurons, respectively [20]. Similar to ADL cilia (Figure 2C), AWB cilia are largely intact in *che-10* L2 mutants (Figure 4B). However, the PCMC area marked by ODR-10::GFP is significantly smaller compared to wild-type (Figures 4B and 4Ci). In addition, ODR-10::GFP shows prominent, abnormal posterior accumulations along dendrites (Figure 4B). Analysis of SRBC-66::GFP in *che-10* L2 mutants reveals shorter, degenerating ASK neuron cilia and phenotypes similar to AWB neurons: a smaller PCMC area and posterior accumulations (Figures 4B and 4Cii). We also assessed the localization of the PCMC/cilia-localized RAB-5 endocytic protein [20]. In *che-10* mutants, RAB-5 shows reduced ciliary localization and increased PCMC accumulation (Figure 4B). Finally, to examine PCMC ultrastructure defects, we examined cross-sections of amphid channel neurons of L2 and young adult *che-10* mutants by TEM as described previously [20]. A significant fraction (14%–28%) of PCMCs exhibit accumulations of membranous or electron-dense material not observed in wild-type worms (Figure 4D; Table S1).

Together, our fluorescent marker and TEM studies reveal marked changes in PCMC structure and organization in cells lacking CHE-10/rootletin. On this basis, we propose that the correct delivery, function, and/or assembly of BB-ciliary components is impaired, eventually leading to the progressive loss of IFT function and degeneration of the axoneme, TZ, and BB.

CHE-10/Rootletin Is Required in Neurons with Striated Rootlets for Avoidance of CO_2

Because CHE-10/rootletin is critical for maintaining amphid and phasmid cilia lacking striated rootlets, we wondered whether it supports IL1/OLQ/BAG cilia that possess striated rootlets. Although these cilia are seemingly intact in *che-10(e1809)* adults ([5]; data not shown), we hypothesized that they might be functionally impaired.

We used an automated worm tracker [21] to assay acute CO_2 avoidance as a readout of rootlet-containing BAG cilia functionality [22]. As expected, wild-type worms react to CO_2 by ceasing forward movement and performing a burst of turns [23, 24] (Figures S3Ai and S3B), and *gcy-9* mutants, which lack the receptor-type guanylate cyclase essential for CO_2 sensation [25], do not (Figures S3Ai and S3B). Next, we tested CO_2 responsiveness of an IFT mutant, *osm-5* (*IFT88* ortholog), which lacks cilia. Although *osm-5* animals respond to CO_2 (Figures S3Ai and S3B), response duration is significantly longer (Figure S3Aii), suggesting that IFT/cilia regulate this aspect of the response. Interestingly, similar to *osm-5* mutants, *che-10* mutants avoid CO_2 (Figures S3Aiii and S3C) and have a significantly prolonged response duration (Figure S3Aiv). Thus, although BAG cilia (which normally have rootlets) appear structurally intact in *che-10* mutants, their functionality is altered.

In sum, our studies reveal that changes in PCMC molecular makeup, organization, and/or function—potentially caused by anomalies in late stages of ciliary trafficking—may provide a viable explanation for the observed IFT defects and progressive degeneration of the axoneme, TZ, and BB upon loss of CHE-10/rootletin. The findings are significant, not only because they provide insights into the general role of rootletin in metazoans but also because they reveal a previously unknown function of nonfilamentous forms of rootletin in ciliary maintenance and function. Future experiments should help clarify how rootletin—for example, by interacting with vesicle trafficking and fusion components and/or the actin cytoskeleton—facilitates vesicular and ciliary trafficking and maintains the integrity of the periciliary membrane, BB, and cilia.

Supplemental Information

Supplemental Information includes three figures, one table, Supplemental Experimental Procedures, and four movies and can be found with this article online at http://dx.doi.org/10.1016/j.cub.2013.08.033.

Acknowledgments

We thank Rex A. Kerr (Howard Hughes Medical Institute, Janelia Farm Research Campus) for technical assistance with the CO_2 behavioral assays. This work was supported by a grant from the Canadian Institutes of Health Research (grant MOP-82870). M.R.L. acknowledges a Senior Scholar Award from the Michael Smith Foundation for Health Research. O.E.B. acknowledges the European Community's Seventh Framework Programme FP7/2009 under grant agreement number 241955, SYSCILIA.

Received: May 16, 2013
Revised: July 20, 2013
Accepted: August 7, 2013
Published: October 3, 2013

References

1. Goetz, S.C., and Anderson, K.V. (2010). The primary cilium: a signalling centre during vertebrate development. Nat. Rev. Genet. *11*, 331–344.
2. Marshall, W.F., Qin, H., Rodrigo Brenni, M., and Rosenbaum, J.L. (2005). Flagellar length control system: testing a simple model based on intraflagellar transport and turnover. Mol. Biol. Cell *16*, 270–278.
3. Yang, J., Liu, X., Yue, G., Adamian, M., Bulgakov, O., and Li, T. (2002). Rootletin, a novel coiled-coil protein, is a structural component of the ciliary rootlet. J. Cell Biol. *159*, 431–440.
4. McClintock, T.S., Glasser, C.E., Bose, S.C., and Bergman, D.A. (2008). Tissue expression patterns identify mouse cilia genes. Physiol. Genomics *32*, 198–206.
5. Perkins, L.A., Hedgecock, E.M., Thomson, J.N., and Culotti, J.G. (1986). Mutant sensory cilia in the nematode *Caenorhabditis elegans*. Dev. Biol. *117*, 456–487.
6. Ou, G., Koga, M., Blacque, O.E., Murayama, T., Ohshima, Y., Schafer, J.C., Li, C., Yoder, B.K., Leroux, M.R., and Scholey, J.M. (2007). Sensory ciliogenesis in *Caenorhabditis elegans*: assignment of IFT components into distinct modules based on transport and phenotypic profiles. Mol. Biol. Cell *18*, 1554–1569.
7. Hao, L., Thein, M., Brust-Mascher, I., Civelekoglu-Scholey, G., Lu, Y., Acar, S., Prevo, B., Shaham, S., and Scholey, J.M. (2011). Intraflagellar transport delivers tubulin isotypes to sensory cilium middle and distal segments. Nat. Cell Biol. *13*, 790–798.
8. Pedersen, L.B., Geimer, S., and Rosenbaum, J.L. (2006). Dissecting the molecular mechanisms of intraflagellar transport in *Chlamydomonas*. Curr. Biol. *16*, 450–459.
9. Silverman, M.A., and Leroux, M.R. (2009). Intraflagellar transport and the generation of dynamic, structurally and functionally diverse cilia. Trends Cell Biol. *19*, 306–316.
10. Starich, T.A., Herman, R.K., Kari, C.K., Yeh, W.H., Schackwitz, W.S., Schuyler, M.W., Collet, J., Thomas, J.H., and Riddle, D.L. (1995). Mutations affecting the chemosensory neurons of *Caenorhabditis elegans*. Genetics *139*, 171–188.
11. Yamamoto, M. (1976). An electron microscopic study of the olfactory mucosa in the bat and rabbit. Arch. Histol. Jpn. *38*, 359–412.
12. Yang, J., Gao, J., Adamian, M., Wen, X.H., Pawlyk, B., Zhang, L., Sanderson, M.J., Zuo, J., Makino, C.L., and Li, T. (2005). The ciliary rootlet maintains long-term stability of sensory cilia. Mol. Cell. Biol. *25*, 4129–4137.
13. Yang, J., and Li, T. (2005). The ciliary rootlet interacts with kinesin light chains and may provide a scaffold for kinesin-1 vesicular cargos. Exp. Cell Res. *309*, 379–389.
14. Bauer, M.C., O'Connell, D.J., Maj, M., Wagner, L., Cahill, D.J., and Linse, S. (2011). Identification of a high-affinity network of secretagogin-binding proteins involved in vesicle secretion. Mol. Biosyst. *7*, 2196–2204.

15. Lanzetti, L. (2007). Actin in membrane trafficking. Curr. Opin. Cell Biol. *19*, 453–458.
16. Snow, J.J., Ou, G., Gunnarson, A.L., Walker, M.R.S., Zhou, H.M., Brust-Mascher, I., and Scholey, J.M. (2004). Two anterograde intraflagellar transport motors cooperate to build sensory cilia on *C. elegans* neurons. Nat. Cell Biol. *6*, 1109–1113.
17. Ou, G., Blacque, O.E., Snow, J.J., Leroux, M.R., and Scholey, J.M. (2005). Functional coordination of intraflagellar transport motors. Nature *436*, 583–587.
18. Engel, B.D., Ludington, W.B., and Marshall, W.F. (2009). Intraflagellar transport particle size scales inversely with flagellar length: revisiting the balance-point length control model. J. Cell Biol. *187*, 81–89.
19. Williams, C.L., Li, C., Kida, K., Inglis, P.N., Mohan, S., Semenec, L., Bialas, N.J., Stupay, R.M., Chen, N., Blacque, O.E., et al. (2011). MKS and NPHP modules cooperate to establish basal body/transition zone membrane associations and ciliary gate function during ciliogenesis. J. Cell Biol. *192*, 1023–1041.
20. Kaplan, O.I., Doroquez, D.B., Cevik, S., Bowie, R.V., Clarke, L., Sanders, A.A., Kida, K., Rappoport, J.Z., Sengupta, P., and Blacque, O.E. (2012). Endocytosis genes facilitate protein and membrane transport in *C. elegans* sensory cilia. Curr. Biol. *22*, 451–460.
21. Swierczek, N.A., Giles, A.C., Rankin, C.H., and Kerr, R.A. (2011). High-throughput behavioral analysis in *C. elegans*. Nat. Methods *8*, 592–598.
22. Hallem, E.A., and Sternberg, P.W. (2008). Acute carbon dioxide avoidance in *Caenorhabditis elegans*. Proc. Natl. Acad. Sci. USA *105*, 8038–8043.
23. Bretscher, A.J., Busch, K.E., and de Bono, M. (2008). A carbon dioxide avoidance behavior is integrated with responses to ambient oxygen and food in *Caenorhabditis elegans*. Proc. Natl. Acad. Sci. USA *105*, 8044–8049.
24. McGrath, P.T., Rockman, M.V., Zimmer, M., Jang, H., Macosko, E.Z., Kruglyak, L., and Bargmann, C.I. (2009). Quantitative mapping of a digenic behavioral trait implicates globin variation in *C. elegans* sensory behaviors. Neuron *61*, 692–699.
25. Hallem, E.A., Spencer, W.C., McWhirter, R.D., Zeller, G., Henz, S.R., Rätsch, G., Miller, D.M., 3rd, Horvitz, H.R., Sternberg, P.W., and Ringstad, N. (2011). Receptor-type guanylate cyclase is required for carbon dioxide sensation by *Caenorhabditis elegans*. Proc. Natl. Acad. Sci. USA *108*, 254–259.